phys. stat. sol. (b) 83, 451 (1977)

Subject classification: 11

Sektion Physik der Humboldt-Universität zu Berlin,
Bereich Atomstoßprozesse der Festkörperphysik

The Energy–Angle Distribution of Heavy Particles Penetrating Solids

By

L. MEYER[1]), M. KLEIN[2]), and R. WEDELL

Particles of definite initial energy and direction penetrating into a solid have, in a given depth, a certain distribution with respect to energy loss and scattering angle. This energy-angle distribution is calculated in small angle approximation for heavy low energy particles, taking scattering and nuclear stopping into account on the basis of a Thomas-Fermi potential and electronic stopping with a definite dependence on scattering angle. Introducing reduced values of energy loss, scattering angle, and thickness of the penetrated layer, it is found, that it is possible to get a general solution independent of particle and target type and of energy. The result is given by a combination of two functions which are tabulated. The most probable energy losses of the total energy distribution and of the distribution of the particles scattered in forward direction as well as the half-widths of these distributions are given. The results show, that stopping and scattering cannot be considered independently for heavy low energy particles. In particular the conception of 'stopping cross section' at low energies essentially looses its meaning.

Teilchen einer gegebenen Einschußenergie und -richtung haben nach Durchdringen einer Festkörperschicht gegebener Dicke eine bestimmte Verteilung in bezug auf ihren Energieverlust und Streuwinkel. Diese Energie–Winkel-Verteilung wird unter Berücksichtigung der Streuung und der Kernbremsung bei Verwendung des Thomas-Fermi-Potentials sowie der elektronischen Bremsung mit einer eindeutigen Abhängigkeit vom Streuwinkel für niederenergetische schwere Teilchen in Kleinwinkelnäherung berechnet. Es zeigt sich, daß bei Einführung reduzierter Variabler für Energieverlust, Streuwinkel und Schichtdicke eine allgemeine Lösung möglich ist, die nicht von Teilchen- und Targettyp oder der Einschußenergie abhängt. Die Verteilung ist als Kombination zweier tabellierter Funktionen dargestellt. Weiterhin sind Tabellen für den wahrscheinlichsten Energieverlust der Gesamtenergieverteilung und der Verteilung von in Vorwärtsrichtung gestreuten Teilchen sowie für die Halbwertsbreiten dieser Verteilungen gegeben. Die Ergebnisse zeigen, daß für niederenergetische schwere Teilchen Bremsung und Streuung nicht als unabhängig voneinander angesehen werden können. Insbesondere verliert deshalb die Konzeption von „Bremsquerschnitten" bei geringen Energien ihren Sinn.

1. Introduction

Particles of given energy and direction which penetrate into a solid are deflected and lose energy. Having passed a definite layer of matter they have a certain distribution with respect to energy and direction which in the following is called energy-angle distribution. Its calculation is of fundamental importance for the investigation of the penetration process of heavy particles. This importance relates only in minor degree to the determination of the spatial distribution of implanted ions but mainly concerns the fundamental characteristics of the stopping process and its experimental investigation. This interrelation can be explained considering, e.g. the stopping cross-

[1]) Present address: Akademie der Wissenschaften der DDR, Zentralinstitut für Optik und Spektroskopie, 1199 Berlin, Rudower Chaussee 6.

[2]) Present address: Akademie der Wissenschaften der DDR, Institut für Hochenergiephysik, 1615 Zeuthen, Plantanenallee 6.

section of low-energy heavy particles and its experimental determination. Usually this quantity is determined as follows. First the energy loss in a thin layer of matter is measured for those particles which have been scattered in forward direction. Analyzing the data it is generally assumed that these particles suffered complete electronic stopping, whereas nuclear stopping was only effective by a certain part which is subtracted by means of more or less motivated corrections (see e.g. [1]). It is assumed then that the quantity determined in this way is an electronic stopping cross-section S_e which can be compared with theoretical values of

$$S_e = \int q_e \, d\sigma \,. \tag{1}$$

Here q_e is the energy transferred to electrons in a collision with a target atom and $d\sigma$ is the differential cross-section for this energy transfer.

The opinion just described is motivated by the assumption that the electronic stopping is a quasi-continuous process which does not essentially depend on the scattering angle. The same idea is inherent in a method developed by Högberg [2]. This author measures energy losses at zero scattering angle for different thicknesses t of material and by extrapolating the measured 'stopping cross-sections' to $t = 0$ he means to separate nuclear stopping from the electronic one. Indeed, this procedure excludes all particles which suffered a substantial deflection (and therefore nuclear stopping). But naturally their electronic stopping is also eliminated. Therefore, the procedure of Högberg yields a stopping cross-section S^* which is attained by limiting the integration in (1) to the range of scattering angles defined by the detector. This stopping cross-section S^* is characteristic of electronic stopping only in the case, where the neglected scattering processes do not essentially contribute to (1), this means if $q_e \, d\sigma$ sufficiently rapidly vanishes with increasing scattering angle. Measurements of the energy loss in single scatterings (see e.g. [3, 4]), however, show, that the energy transfer to electrons is rapidly increasing with increasing scattering angle.

2. Calculation of the Energy–Angle Distribution

Therefore, the interpretation of stopping cross-sections determined according to the procedures explained above is an open question. To clarify this question a detailed analysis of the energy-angle distribution is necessary.

The analytic calculation of the energy–angle distribution is taken from an unpublished investigation [5] which is based on the same fundamental assumptions as the theory of ordinary multiple scattering of low-energy heavy particles [6], which has proved its usefulness in many experimental investigations. This calculation starts from the interaction potential

$$V(r) = \frac{Z_1 Z_2 e^2}{r} \varphi\left(\frac{r}{a}\right) \tag{2}$$

and the resulting differential scattering cross-section given in the form originally used by Lindhard et al. [7]

$$\frac{d\sigma}{d\eta} = \pi a^2 \frac{f(\eta)}{\eta^2} \,. \tag{3}$$

Here Z_1 and Z_2 are the atomic numbers of the incident and target particles. The function φ and the screening parameter a serve to characterize the screening effect of the electron shells. The characteristic function $f(\eta)$ of the cross-section has been tabulated in [6, 7] for several screening functions. The reduced scattering angle η in small-angle approximation is related to the scattering angle χ in the laboratory frame

by

$$\eta = \frac{\varepsilon}{2} \frac{m_1 + m_2}{m_2} \chi \,. \tag{4}$$

Here m_1 and m_2 are the masses of the projectile and target particles, respectively. The reduced energy ε is proportional to the energy E of the incident particles according to

$$\varepsilon = \frac{a}{Z_1 Z_2 e^2} \frac{m_2}{m_1 + m_2} E \,, \tag{5}$$

where e is the elementary charge.

The process of penetration into the solid is considered to be a sequence of two-particle collisions. Therefore, as was done in [6], the effect of the potential (2) or more precisely the scattering cross-section (3) in a solid of atomic number density N is confined to a spherical volume of radius r_0, which is given by

$$r_0 = \frac{1}{2} N^{-1/3} \,. \tag{6}$$

This limitation determines a minimum single-scattering angle η_0 by the relation

$$\int_{\eta_0}^{\varepsilon} \frac{\mathrm{d}\sigma}{\mathrm{d}\eta} \mathrm{d}\eta = \pi r_0^2 \,. \tag{7}$$

From the total scattering cross-section πr_0^2 we get the mean number of collisions n in a layer of thickness t of an amorphous or very finely crystalline solid

$$n = \pi r_0^2 N t = \frac{\pi}{4} N^{1/3} t \,. \tag{8}$$

As $2r_0$ corresponds to the distance of neighbouring atoms and as the density in a solid even in microscopically small dimensions hardly fluctuates (in contrast to the behaviour of a gas), the fluctuations of the collision number around the mean value (8) are very small.

The energy loss $q(\chi)$ can easily be calculated from energy–momentum conservation. In small-angle approximation follows

$$q_\mathrm{n}(\chi) = \frac{m_1}{m_2} E \chi^2 = c_\mathrm{n} \eta^2 \,, \tag{9a}$$

where

$$c_\mathrm{n} = \frac{4}{\varepsilon} \frac{m_1}{m_1 + m_2} \frac{Z_1 Z_2 e^2}{a} = \frac{4}{E} \frac{m_1}{m_2} \left(\frac{Z_1 Z_2 e^2}{a} \right)^2 . \tag{9b}$$

For the electronic energy loss ascribed to a single collision the following ansatz is used:

$$q_\mathrm{e}(\chi) = c_{\mathrm{e}_0} + c_{\mathrm{e}_2} \eta^2 + c_{\mathrm{e}_4} \eta^4 + \ldots \,. \tag{10}$$

In continuation of the small-angle approximation the following calculation is restricted to the first two terms of (10). The first term c_{e_0} corresponds to the stopping at zero scattering angle typical for solids. Odd powers of η in (10) are neglected for symmetry reasons. From (9) and (10) we get the total energy loss in a single collision

$$q(\chi) = q_\mathrm{e}(\chi) + q_\mathrm{n}(\chi) = c_{\mathrm{e}_0} + (c_{\mathrm{e}_2} + c_\mathrm{n}) \eta^2 + \ldots \,. \tag{11}$$

In the following calculation it is assumed that the energy loss $q(\chi)$ is uniquely determined by the scattering angle, i.e., (11) is valid not only in the average but in every single collision. This assumption is certainly justified with respect to the elastic energy loss $q(\chi)$. For the electronic energy loss it is, however, only an approximation which is satisfied the better the more electrons take part in the energy exchange. Measurements of Bierman et al. [8, 4], for example, have shown that the electronic energy loss in a single collision of different incident particles with neon and argon atoms at fixed scattering angle is not uniquely defined, but its dispersion remains smaller than the total energy loss and the average electronic energy loss is a monotonously increasing function of the scattering angle. The same state of affairs can also be seen from the measurements of Kessel and Everhart [9].

Denoting by $F_1(\chi, q)$ the probability distribution after one collision of a particle with the deflection χ in the solid angle $\mathrm{d}\omega$ and an energy loss between q and $q + \mathrm{d}q$ we have

$$F_1(\chi, q)\,\mathrm{d}\omega\,\mathrm{d}q = \mathrm{d}\omega\,\mathrm{d}q \begin{cases} \dfrac{1}{\pi r_0^2}\dfrac{\mathrm{d}\sigma}{\mathrm{d}\omega}\,\delta(q - q(\chi)) & \eta \geqq \eta_0\,, \\ 0 & \eta \leqq \eta_0\,, \end{cases} \tag{12}$$

where $\delta(q - q(\chi))$ is Dirac's delta function.

For the differential cross-section $\mathrm{d}\sigma/\mathrm{d}\omega$ we get from (3) and (4)

$$\frac{\mathrm{d}\sigma}{\mathrm{d}\omega} = \frac{\varepsilon^2}{8}\,a^2\left(\frac{m_1 + m_2}{m_2}\right)^2 \frac{f(\eta)}{\eta^3}\,. \tag{13}$$

The energy losses $q_i(\chi)$ and the deflections $\boldsymbol{\chi}_i$ of the subsequent collisions ($i = 1, 2, \ldots, n$) yield the total energy loss

$$Q = \sum_{i=1}^{n} q_i \tag{14}$$

and the total scattering angle

$$\boldsymbol{\vartheta} = \sum_{i=1}^{n} \boldsymbol{\chi}_i\,. \tag{15}$$

Here the different azimuthal directions of the scattering angles $\boldsymbol{\chi}_i$ are taken into account in small-angle approximation by vector addition of the scattering angles in a plane perpendicular to the initial direction.

Now, the energy-angle distribution after n collisions is related to the distribution after $n - 1$ collisions by the equation

$$F_n(\vartheta, Q)\,\mathrm{d}\omega\,\mathrm{d}Q = \mathrm{d}\omega\,\mathrm{d}Q \int_0^\infty \int_0^{2\pi} \int_0^\infty F_{n-1}(\boldsymbol{\vartheta} - \boldsymbol{\chi}, Q - q)\,F_1(\chi, q)\,\mathrm{d}\omega_\chi\,\mathrm{d}q\,. \tag{16}$$

The integration is extended over the elements of area $\mathrm{d}\omega_\chi$ pertaining to the angle $\boldsymbol{\chi}$ in the plane of the $\boldsymbol{\chi}$-vectors and over the corresponding energy losses q. From this expression we get, using a Hankel-Fourier transformation (see [5]) and neglecting the energy dependence of $\mathrm{d}\sigma/\mathrm{d}\omega$ and $q(\chi)$

$$F_n(\vartheta, Q) = \frac{\varepsilon^2}{(4\pi)^2}\,\frac{1}{c_{e_2} + c_n}\left(\frac{m_1 + m_2}{m_2}\right)^2 \times$$

$$\times \int_{-\infty}^{+\infty} \int_0^\infty G_1^n(z, w)\,J_0(z\tilde{\vartheta})\,\mathrm{e}^{-iw[(\tilde{Q} + nc_{e_0})/(c_{e_2} + c_n)]}\,z\,\mathrm{d}z\,\mathrm{d}w\,, \tag{17}$$

where

$$G_1(z, w) = \frac{a^2}{r_0^2} e^{iwc_{e_0}/(c_{e_2}+c_n)} \int_{\eta_0}^{\infty} \frac{f(\eta)}{\eta^2} J_0(z\eta)\, e^{iw\eta^2}\, d\eta .$$

J_0 is the Bessel function of zero order and

$$\tilde{\vartheta} = \vartheta \frac{\varepsilon}{2} \frac{m_1 + m_2}{m_2}, \tag{18}$$

$$\tilde{Q} = \frac{Q - nc_{e_0}}{c_{e_2} + c_n} \tag{19}$$

are reduced scattering angle and reduced energy loss, respectively. As in the theory of multiple scattering [6] we define a function

$$\Delta(z, w) = \frac{r_0^2}{a^2}[1 - e^{-iwc_{e_0}/(c_{e_2}+c_n)} G_1(z, w)]$$

$$= \int_{\eta_0}^{\infty} \frac{f(\eta)}{\eta^2}[1 - J_0(z\eta)\, e^{iw\eta^2}]\, d\eta . \tag{20}$$

In this integral the integrand behaves like $f(\eta)\,[z^2/4 - iw]$ for small values of η. Therefore, as with the angular distribution [6], the lower limit of integration η_0 can be replaced by zero. This is correct up to large values of z and w ($z > 50$, $|w| > 500$). which are important only at extremely small thicknesses of material. In this region of not extremely large values of z and w the relation holds $|a^2/r_0^2\, \Delta(z, w)| \ll 1$. Therefore, we can expand $[1 - a^2/r_0^2\, \Delta]^n$ in series and get from (20)

$$G_1^n(z, w) = e^{iwnc_{e_0}/(c_{e_2}+c_n)}\, e^{-\tau\Delta}\left[1 - \frac{1}{2}\frac{a^2}{r_0^2}\tau\Delta^2 + \ldots\right], \tag{21}$$

where

$$\tau = \pi a^2 N t \tag{22}$$

is the reduced thickness.

Thus we finally get the energy–angle distribution

$$F_n(\vartheta, Q)\, d\omega\, dQ = \frac{d\omega\, dQ}{(4\pi)^2} \frac{\varepsilon^2}{c_{e_2} + c_n} \left(\frac{m_1 + m_2}{m_2}\right)^2 \left[f_1(\tau, \tilde{\vartheta}, \tilde{Q}) - \frac{a^2}{r_0^2} f_2(\tau, \tilde{\vartheta}, \tilde{Q}) + \ldots\right], \tag{23}$$

where

$$f_1(\tau, \tilde{\vartheta}, \tilde{Q}) = \int_0^{\infty} \int_{-\infty}^{+\infty} e^{-\tau\Delta(z,w) - iw\tilde{Q}} J_0(z\tilde{\vartheta})\, dw\, z\, dz \tag{23a}$$

and

$$f_2(\tau, \tilde{\vartheta}, \tilde{Q}) = \frac{\tau}{2} \int_0^{\infty} \int_{-\infty}^{+\infty} e^{-\tau\Delta(z,w) - iw\tilde{Q}} J_0(z\tilde{\vartheta})\, \Delta^2(z, w)\, dw\, z\, dz . \tag{23b}$$

An estimation of the integrals f_1 and f_2 (see [10]) shows that, as with the pure angular distribution [6], $(a^2/r_0^2)\, f_2$ is only a small correction to f_1, which is only of importance at very small thicknesses (see [10]).

In [10] it has been verified that in the limiting case of large values of τ energy and angle distributions become independent of each other and both have a Gaussian behaviour.

Integrating the distribution $F_n(\vartheta, Q)$ over all scattering angles one gets the total energy distribution

$$F_n(Q)\,\mathrm{d}Q = \frac{\mathrm{d}Q}{2\pi(c_{e_2} + c_n)}\left[f_1(\tau, \tilde{Q}) - \frac{a^2}{r_0^2} f_2(\tau, \tilde{Q}) + \ldots\right], \tag{24}$$

where

$$f_1(\tau, \tilde{Q}) = \int_{-\infty}^{+\infty} \mathrm{e}^{-\tau\Delta(0,w) - iw\tilde{Q}}\,\mathrm{d}\omega\,, \tag{24a}$$

$$f_2(\tau, \tilde{Q}) = \frac{\tau}{2}\int_{-\infty}^{+\infty} \mathrm{e}^{-\tau\Delta(0,w) - iw\tilde{Q}}\,\Delta^2(0, w)\,\mathrm{d}w\,. \tag{24b}$$

The corresponding integration of $F_n(\vartheta, Q)$ (23) over the energy losses results in the total angle distribution already calculated in [6].

Equations (23) and (24) allow to draw some general conclusions: The shape of the energy distribution (at a fixed scattering angle by integrating over all angles) and the position of its maximum, represented by the reduced variable $\tilde{Q}$, do not depend on energy, mass and atomic number of the particles and are essentially determined by the reduced thickness τ and the scattering angle ϑ. The experimentally measured most probable energy loss

$$Q_m = (c_{e_2} + c_n)\,\tilde{Q}_m + nc_{e_0} = (c_{e_2} + c_n)\,\tilde{Q}_m(\tau) + \frac{r_0^2}{a^2} c_{e_0}\tau \tag{25}$$

consists of two terms with different functional dependence on the thickness of material. Thus it should be possible to separate both terms experimentally and to determine the constants c_{e_0} and c_{e_2}. In the case of $c_{e_2} \ll c_n$ this separation is simultaneously a separation of nuclear stopping and electronic stopping. The part of the measured most probable energy loss Q_{m_n} which is determined by the nuclear stopping $Q_{m_n} = c_n\tilde{Q}_m = \frac{4}{E}\frac{m_1}{m_2}\frac{Z_1 Z_2 e^2}{a}\tilde{Q}_m$ is proportional to the inverse of the energy of the incident particles in contrast to the so-called nuclear stopping cross-section $S_n = \int q_n\,\mathrm{d}\sigma$ which has a slightly different energy dependence (see [11]). This difference is explained by the deviating energy dependence of the tail of the energy distribution which is not included in the preceding calculation. The experimentally measured half-width of the energy distribution

$$Q_{1/2} = (c_{e_2} + c_n)\,\tilde{Q}_{1/2} \tag{26}$$

is also proportional to E^{-1} in the case $c_{e_2} \ll c_n$, whereas the average square fluctuation of the energy loss $(Nt\Omega^2)^{1/2} = (Nt\int q_n^2\,\mathrm{d}\sigma)^{1/2}$ has a different dependence on the energy. Corresponding general conclusions concerning the angular distribution have already been given in [6].

3. Numerical Results

Excluding extremely small reduced thicknesses τ the energy–angle distribution is mainly determined by the function $f_1(\tau, \tilde{\vartheta}, \tilde{Q})$ (23a). This function has been calculated numerically in the region $0.6 \leqq \tau \leqq 15$.

Starting from the scattering cross-section (3) with $f(\eta)$ calculated for the Thomas-Fermi screening function, at first the real and imaginary parts of the function $\Delta(z, w)$

were determined according to (20). Then as a first step in the calculation of f_1 according to (23a) the integration over w was done, thereby getting the function

$$H(\tau, z, \tilde{Q}) = 2 \int_0^\infty \mathrm{e}^{-\tau \mathrm{Re}\, \Lambda} \cos(\tau \,\mathrm{Im}\, \Lambda + w\tilde{Q})\, \mathrm{d}w \,.$$

A detail examination of this function [10] revealed that it can be approximated by

$$H(\tau, z, \tilde{Q}) = A(\tau, \tilde{Q})\, \mathrm{e}^{-B(\tau, \tilde{Q}) z^2} \tag{27}$$

up to a maximum value $\tilde{Q}_0 \approx 5\tilde{Q}_\mathrm{m}(0)$ where $\tilde{Q}_\mathrm{m}(0)$ is the most probable energy loss at $\vartheta = 0$.

$$f_1(\tau, \tilde{\vartheta}, \tilde{Q}) = \frac{A(\tau, \tilde{Q})}{2B(\tau, \tilde{Q})} \exp\left[-\frac{\tilde{\vartheta}^2}{4B(\tau, \tilde{Q})}\right]. \tag{28}$$

The total energy distribution according to (24a) turns out to be

$$f_1(\tau, \tilde{Q}) = \int_0^\infty f_1(\tau, \vartheta, \tilde{Q})\, \tilde{\vartheta}\, \mathrm{d}\vartheta = A(\tau, \tilde{Q}) \,. \tag{29}$$

The coefficients $A(\tau, \tilde{Q})$ and $B(\tau, \tilde{Q})$ have been calculated by a fit to the numerically given function $H(\tau, z, \tilde{Q})$. The result is given in Table 1, 2, and 3. For simplicity the coefficients were normalized to the values $A(\tau, \tilde{Q})_\mathrm{m} = A_\mathrm{m}(\tau)$ and $B(\tau, \tilde{Q}_\mathrm{m}) = B_\mathrm{m}(\tau)$ at the most probable energy loss $\tilde{Q}_\mathrm{m}$.

The Gaussian behaviour of the angular distribution (28) at relatively small values of Q, and therefore the possibility of the approximation (27), can be explained as

Table 1

The ratio $A(\tau, \tilde{Q})/A_\mathrm{m}(\tau)$ as a function of the reduced thickness τ and the normalized energy loss $\tilde{Q}/\tilde{Q}_\mathrm{m}$

$\tilde{Q}/\tilde{Q}_\mathrm{m}$	τ										
	0.6	0.8	1.0	1.5	2.0	3.0	4.0	6.0	8.0	10	15
0.2	0.0	0.1	0.1	0.03	0.02	0.01	0.01	0.00	0.00	0.00	0.00
0.3	0.1	0.2	0.22	0.16	0.11	0.07	0.05	0.04	0.03	0.02	0.01
0.4	0.3	0.41	0.41	0.35	0.29	0.24	0.22	0.19	0.17	0.15	0.13
0.5	0.56	0.60	0.61	0.57	0.52	0.47	0.45	0.41	0.39	0.37	0.34
0.6	0.73	0.75	0.76	0.74	0.72	0.69	0.67	0.65	0.63	0.61	0.59
0.7	0.86	0.87	0.87	0.86	0.85	0.85	0.84	0.83	0.82	0.81	0.80
0.8	0.94	0.95	0.95	0.95	0.95	0.94	0.94	0.93	0.93	0.93	0.92
1.0	1.00	1.00	1.00	1.00	1.00	1.00	1.00	1.00	1.00	1.00	1.00
1.2	0.98	0.98	0.98	0.97	0.97	0.97	0.96	0.96	0.95	0.95	0.94
1.4	0.92	0.92	0.92	0.91	0.91	0.89	0.88	0.86	0.84	0.83	0.80
1.6	0.86	0.87	0.87	0.85	0.84	0.81	0.79	0.75	0.73	0.71	0.67
1.8	0.80	0.80	0.80	0.78	0.76	0.73	0.70	0.66	0.63	0.60	0.56
2.0	0.74	0.75	0.74	0.72	0.69	0.65	0.62	0.57	0.54	0.51	0.46
2.5	0.60	0.61	0.60	0.57	0.54	0.49	0.45	0.40	0.37	0.34	0.29
3.0	0.49	0.50	0.49	0.46	0.43	0.38	0.34	0.30	0.26	0.24	0.20
3.5	0.41	0.42	0.41	0.38	0.34	0.30	0.26	0.22	0.19	0.16	0.12
4.0	0.35	0.36	0.35	0.32	0.29	0.24	0.21	0.17	0.14	0.12	0.08

Table 2

The ratio $B(\tau, \tilde{Q})/B_m(\tau)$ as a function of the normalized energy loss $\tilde{Q}/\tilde{Q}_m$

$\tilde{Q}/\tilde{Q}_m$	B/B_m	$\tilde{Q}/\tilde{Q}_m$	B/B_m
0.2	0.2	1.6	1.66
0.4	0.40	1.8	1.88
0.6	0.60	2.0	2.10
0.8	0.80	2.5	2.67
1.0	1.00	3.0	3.24
1.2	1.21	3.5	3.77
1.4	1.43	4.0	4.25

Table 3

The quantities $\tilde{Q}_m$, A_m, and B_m as functions of the reduced thickness, complemented by values of $\tilde{Q}_{1/2}$, $\tilde{Q}_m(0)$, and $\tilde{Q}_{1/2}(0)$.

$\tilde{Q}_m$ most probable reduced energy loss of the total energy distribution, $A_m = A(\tilde{Q}_m)$, $B_m = B(\tilde{Q}_m)$, $\tilde{Q}_m(0)$ most probable energy loss at the scattering angle $\tilde{\vartheta} = 0$, $\tilde{Q}_{1/2}$ reduced half-width of the total energy distribution, $\tilde{Q}_{1/2}(0)$ reduced half-width of the energy distribution at the scattering angle $\tilde{\vartheta} = 0$

τ	$\tilde{Q}_m$	A_m	B_m	$\tilde{Q}_{1/2}$	$\tilde{Q}_m(0)$	$\tilde{Q}_{1/2}(0)$
0.6	0.036	40	0.010	0.089	0.023	0.040
0.7	0.047	30	0.013	0.118	0.029	0.052
0.8	0.059	24	0.017	0.150	0.037	0.067
1.0	0.090	16.2	0.026	0.226	0.057	0.102
1.2	0.125	12.1	0.037	0.307	0.080	0.140
1.5	0.188	8.50	0.056	0.440	0.123	0.205
2.0	0.321	5.50	0.093	0.693	0.217	0.341
2.5	0.470	4.05	0.136	0.960	0.327	0.489
3.0	0.645	3.16	0.184	1.26	0.455	0.658
3.5	0.840	2.56	0.237	1.58	0.598	0.848
4.0	1.05	2.11	0.294	1.91	0.754	1.06
5.0	1.52	1.56	0.426	2.63	1.10	1.49
6.0	2.03	1.24	0.569	3.37	1.48	1.96
7.0	2.59	1.02	0.720	4.14	1.90	2.48
8.0	3.16	0.865	0.896	4.93	2.34	3.01
10	4.40	0.672	1.29	6.51	3.28	4.10
12	5.65	0.555	1.70	8.04	4.25	5.20
14	7.00	0.474	2.13	9.56	5.28	6.37
15	7.65	0.448	2.39	10.3	5.80	6.94

follows: According to (19) $\tilde{Q}$ is a measure of the angle-dependent part of the energy loss. In a single collision small contributions to this part of the energy loss are connected to small-angle deflections. As the total energy loss is given by the sum of the absolute values of the single energy losses, small total energy losses Q can only be a result of small single deflections which yield a Gaussian angular distribution. Because the angle-independent part of the electronic stopping is generally larger than the angle-depend-

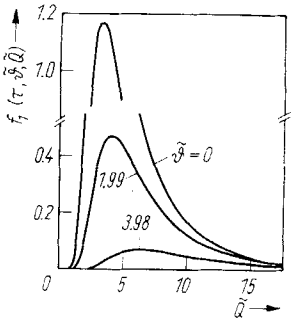

Fig. 1. Energy-angle distributions $f_1(\tau, \tilde{\vartheta}, \tilde{Q})$ for the reduced thickness $\tau = 10$ at the reduced scattering angles $\tilde{\vartheta} = 0$, $\tilde{\vartheta} = \tilde{\vartheta}_{1/2} = 1.99$ and $\tilde{\vartheta} = 2\tilde{\vartheta}_{1/2} = 3.98$ as a function of Q

ent part at small scattering angles, real angular distributions are expected to have such a Gaussian behaviour up to higher total energy losses. This expectation is confirmed, e.g., by experiments of Högberg et al. [12].

The half-width of the angular distribution at a given energy loss Q can easily be calculated from (28)

$$\tilde{\vartheta}_{1/2}(\tau, \tilde{Q}) = 2(B(\tau, \tilde{Q}) \ln 2)^{1/2} . \tag{30}$$

This means that $\vartheta_{1/2}(\tilde{Q})$ is approximately proportional to $\tilde{Q}^{1/2}$ because according to Table 2, $B(\tau, \tilde{Q})$ is linearly increasing with increasing energy loss. Thus the restriction of the Gaussian approximation to $\tilde{Q}$ values smaller than $5\tilde{Q}_m(0)$ corresponds to an upper limit for the half-width $\tilde{\vartheta}_{1/2} \leqq 2[B(\tau, 5\tilde{Q}_m(0)) \ln 2]^{1/2}$. Within this $[\tilde{\vartheta}, \tilde{Q}]$-region (28) is a useful approximation of $f_1(\tau, \tilde{\vartheta}, \tilde{Q})$ with an error restricted to 10% at the ends of the considered region.

As an example the energy–angle distribution for $\tau = 10$ is represented in Fig. 1 by a family of energy distributions at different constant scattering angles. With using scattering angle the maximum of the energy distribution is shifted to larger values of Q, and at the same time the half-width is considerably increasing.

As can be seen from Table 3, the most probable energy loss $\tilde{Q}_m$ of the total energy distribution is increasing with rising thickness τ. This increase is, especially at small thickness, very much stronger than linear. The same is true for the most probable energy loss $\tilde{Q}_m(0)$ at the constant scattering angle $\vartheta = 0$. Thus, according to the present calculation, it is impossible on the basis of the most probable energy losses to get a stopping cross-section which is independent of the thickness τ in the range of thicknesses considered here.

4. Comparison with Other Calculations

Recently Hvelplund [13] calculated energy distributions for pure nuclear stopping on the basis of Landau's method of calculation [14], using, however, Lindhard's scattering cross-section (3) as has been done in the present calculation. He arrives at a total energy distribution in the form

$$f_H\left(\tau, \frac{\gamma}{\varepsilon}\tilde{Q}\right) \mathrm{d}\left(\frac{\gamma}{\varepsilon}\tilde{Q}\right) = \frac{\mathrm{d}\left(\frac{\gamma}{\varepsilon}\tilde{Q}\right)}{\pi} \int_0^\infty \mathrm{e}^{-\tau A_H(y)} \cos\left[y\frac{\gamma}{\varepsilon}Q - \tau C_H(y)\right] \mathrm{d}y , \tag{31}$$

where

$$A_{\mathrm{H}}(y) = \int_0^{\varepsilon} 2 \sin^2\left(\frac{\gamma\eta^2}{2\varepsilon} y\right) \frac{f(\eta)}{\eta^2} \, \mathrm{d}\eta \,, \tag{31a}$$

$$C_{\mathrm{H}}(y) = \int_0^{\varepsilon} \left(\sin \frac{\gamma\eta^2}{\varepsilon} y\right) \frac{f(\eta)}{\eta^2} \, \mathrm{d}\eta \,, \qquad \text{and} \qquad \gamma = \frac{4m_1 m_2}{(m_1 + m_2)^2}. \tag{31b}$$

This distribution is identical with the total energy distribution (24) of the present calculation, if electronic stopping is neglected ($c_{e_0} = c_{e_2} = 0$), if the term $a^2/r_0^2 f_2(\tau, Q)$ is neglected, and if the upper limit of integration ε in (31a) and (31b) is replaced by ∞. In this case the following equations are valid:

$$A_{\mathrm{H}}(y) = \mathrm{Re}\, \Delta\left(0, \frac{\gamma}{\varepsilon} y\right) \qquad \text{and} \qquad C_{\mathrm{H}}(y) = -\,\mathrm{Im}\, \Delta\left(0, \frac{\gamma}{\varepsilon} y\right).$$

The essential difference between the energy distributions (23) and (31) is therefore the different choice of the upper limit of integration in the function $\Delta(0, w)$ (20). In the present calculation the limit ε was replaced immediately by ∞ because, in consequence of the rapide decrease of the differential scattering cross-section, there is generally only a negligible contribution to the integral (20) from the region $\eta > \varepsilon$. Only this replacement gives the possibility for a general computation of the energy–angle distribution which is valid for all energies, as the remaining energy dependence can be expressed by the reduced energy loss and the reduced scattering angle. Hvelplund's paper [13] however calls attention to the fact, that in the special case of heavy ions penetrating hydrogen, such extremely small values of ε may be of practical importance, that the replacement of the upper limit of integration by ∞ will cause substantial errors. We have therefore, examined at which energy $\varepsilon = \varepsilon_{10\%}$ the replacement discussed above will cause a deviation of 10% in the intensity of the maximum of the total energy distribution. The result is given in Table 4.

Table 4

$\varepsilon_{10\%}$ as a function of τ

τ	0.6	0.8	1.0	2	4	6	8	10	15
$\varepsilon_{10\%}$	1.0	1.2	1.3	2.0	2.9	3.7	4.3	4.8	6

For $\varepsilon > \varepsilon_{10\%}$ the deviations in the vicinity of the maximum are smaller than 10%. For $\varepsilon < \varepsilon_{10\%}$ at first the intensity at the maximum of the energy distribution (31) further increases at the expense of the intensity in the tail, and for still further decreasing ε the maximum is finally shifted to smaller energy losses and the half-width diminishes. The values of Table 4, however, show that these deviations only occur at such low energies, which in general are already excluded by the presumption of small energy losses (in relation to the primary energy) in the case of solid targets.

Similar deviations at low energies also occur in the angular distributions. The corresponding energies $\varepsilon_{10\%}$, at which the intensity in the maximum of the total angular distribution deviates by 10% from the values calculated in [6], nearly coincide with the values given in Table 4.

5. Comparison with Experimental Results

The calculation given above contains the constants c_{e_0} and c_{e_2}, which at present can only be determined from experiment. Thus a comparison with single energy distributions is not very affirmative. We therefore restrict the comparison to experiments which include the angular dependence of the energy distributions.

Högberg, et al. [12] investigated the energy distributions of nitrogen ions of 40 keV initial energy having passed a carbon layer of 5.7 $\mu g/cm^2$ ($\tau = 2.8$) at the scattering angles $\vartheta = 0°$ and $\vartheta = 9°$ ($\tilde{\vartheta} = 0.79$). Fig. 2 shows the experimental distributions in comparison with theoretical curves determined from (28) and Tables 1, 2, and 3. The mean energy of the particles was assumed to be 34.5 keV ($\varepsilon = 4.66$). The constants c_{e_0} and c_{e_2} were determined by fitting the theoretical energy distribution at $\vartheta = 0$ to the experimental most probable energy loss and to the experimental half-width. The result was $c_{e_0} = 0.081$ keV and $c_{e_2} = 3.02$ keV.

According to (9b) the nuclear stopping constant c_n is equal to 1.56 keV. As shown in Fig. 2 the theoretical calculation reproduces the most probable energy loss at $\vartheta = 9°$, i.e. the shift of the distribution to higher energy losses at increasing angles. However, the relative intensity and the shape of the distributions significantly deviate. This deviation may partially be due to the energy dependence of the detector used by Högberg and coworkers (current measurement with an open Bendix multiplier) which is responsible for an intensity too small at lower and too high at higher energies.

In the same experiment Högberg and coworkers also investigated the angular distributions at fixed energy loss, which are of Gaussian shape with the half-width's given in Table 5. For comparison the theoretical values according to (30) are included,

Table 5

Q	10 keV	10.9 keV	11.3 keV
$\vartheta_{1/2}$ exp.	7.5°	8.6°	9.9°
$\vartheta_{1/2}$ theor.	6.4°	7.8°	8.4°

using the constants c_{e_0} and c_{e_2} determined above. All theoretical half-widths are slightly smaller than the experimental values.

In another work [2] Högberg investigated "stopping cross-sections" of particles scattered in forward direction in dependence on the thickness of the penetrated layer. For the case of N^+ ions with 34.5 keV mean energy penetrating carbon layers of

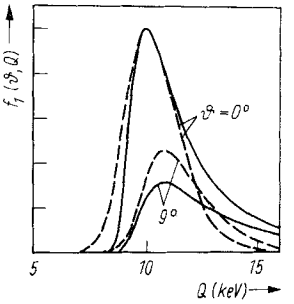

Fig. 2. Energy distributions of nitrogen ions with initial energy of 40 keV after penetrating a carbon layer of a thickness of 5.7 $\mu g/cm^2$ at the scattering angles $\vartheta = 0°$ and 9°. Experimental results (dashed curves) from Högberg et al. [12], theoretical curves (solid) from (28)

different thicknesses, his results are given in Fig. 4 together with a theoretical curve computed from the most probable energy loss $\tilde{Q}_m(0)$ of Table 3 using the constants c_{e_0} and c_{e_2} determined above. The curves agree very well up to a thickness of 7 $\mu g/cm^2$. At this thickness the experimental curve shows a kink and remains constant for larger thicknesses whereas the theoretical curve continues to increase. The reason for this kink in the experimental curve is not clear. It should be mentioned, however, that the theoretical curve refers to the most probable energy loss whereas Högberg uses the mean energy loss which, on account of the uncertainties in the tail of the energy distribution, is difficult to determine experimentally.

In the same paper [2] Högberg presents an energy-angle distribution for the same projectile-target combination at approximately the same mean energy. This distribution cannot be reproduced satisfactorily from the present theory using the constants c_{e_0} and c_{e_2} determined above. It is, however, a striking feature of this distribution (Fig. 1 in [2]) that its corresponding mean energy loss in forward direction is incompatible with the "stopping cross-section" at zero scattering angle and the corresponding thickness as follow from Fig. 2d of the same work. Thus, the presentation of Högbergs results seems to be incorrect.

Ormrod and Duckworth [15] measured the energy distributions of neon ions with 35 keV initial energy having passed a 3.36 $\mu g/cm^2$ carbon layer ($\tau = 1.46$) at four scattering angles ($\vartheta = 0.075, 0.125, 0.175, 0.225$). The results are compared with the theoretical curves according to (23) and Table 1, 2, and 3 in Fig. 3, assuming the mean energy of particles to be 32.5 keV ($\varepsilon = 2.38$). The constants of electronic stopping c_{e_0} and c_{e_2} were determined to be $c_{e_0} = 0.045$ keV and $c_{e_2} = 3.65$ keV whereas c_n according to (9b) is equal to 5.51 keV. With these constants the shape of the ex-

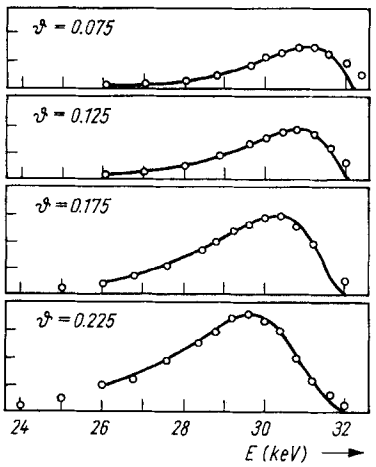

Fig. 3

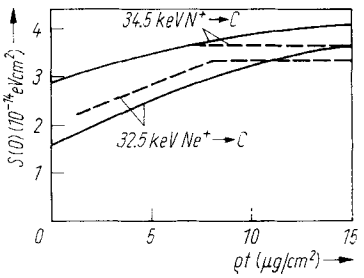

Fig. 4

Fig. 3. Energy distributions of neon ions with initial energy of 35 keV after penetration through a carbon layer of 3.36 $\mu g/cm^2$ thickness at the scattering angles $\vartheta = 0.075, 0.125, 0.175, 0.225$. Experimental points from Ormrod and Duckworth [15], theoretical curves from (28)

Fig. 4. Dependence of the stopping cross sections $S(0)$ on the thickness for particles, scattered in the forward direction in the case of penetration of 34.5 keV nitrogen ions and of 32.5 keV neon ions through carbon layers. Experimental curves (dashed) from Högberg [2] theoretical curves from Table 3

perimental distributions and the shift of the most probable energy loss is reproduced quite well. Unfortunately the experimental distributions at different angles are not normalized to the same number of incident particles. Thus the theoretical curves had to be additionally fitted to the height of the maximal experimental value.

For the case 32.5 keV $Ne^+ \rightarrow C$ just discussed we have also calculated the "stopping cross-section" in forward direction, using the constants c_{e_0} and c_{e_2} determined above. The comparison with experimental results of Högberg [2] is shown in Fig. 4. At small thicknesses the theoretical curve is below the experimental one. This should be expected because the theoretical "stopping cross-section" was calculated with the most probable energy loss in contrast to Högberg who uses the mean energy loss. The bend of the experimental curve at $t = 8\,\mu g/cm^2$, however, is also in this case difficult to understand.

References

[1] B. Fastrup, P. Hvelplund, and C. A. Sautter, Kong. Danske Vid. Selsk., mat.-fys. Medd. **35**, No. 10 (1966).
[2] G. Högberg, phys. stat. sol. (b) **48**, 829 (1971).
[3] V. V. Afrosimov, S. V. Bobashev, Ju. S. Gordejev, and W. M. Lawpov, Zh. eksper. teor. Fiz. **62**, 61 (1972).
[4] D. J. Bierman and D. Van Vliet, Physica **57**, 221 (1972).
[5] L. Meyer, Dissertation B, Humboldt-Universität Berlin 1976.
[6] L. Meyer, phys. stat. sol. (b) **44**, 253 (1971).
[7] J. Lindhard, V. Nielsen, and M. Scharff, Kong. Danske Vid. Selsk., mat.-fys. Medd. **38**, No. 10 (1968).
[8] D. J. Bierman, W. C. Turkenburg, and C. R. Bhalla, Physica **60**, 357 (1972).
[9] Q. C. Kessel and E. Everhart, Phys. Rev. **146**, 16 (1966).
[10] M. Klein and R. Wedell, Diplomarbeit, Humboldt-Universität Berlin 1973.
[11] J. Lindhard, M. Scharff, and H. E. Schiott, Kong. Danske Vid. Selsk., mat.-fys. Medd. **33**, No. 14 (1963).
[12] G. Högberg, H. Norden, and H. G. Berry, Nuclear Instrum. and Methods **90**, 283 (1970).
[13] P. Hvelplund, Phys. Rev. A **11**, 1921 (1975).
[14] L. Landau, J. Phys. (USSR) **8**, 201 (1944).
[15] J. Ormrod and H. Duckworth, Canad. J. Phys. **41**, 1424 (1963).

(Received July 18, 1977)